

Acousto-Optic Beam Steering IDT Design with ScAlN

Elizabeth Mountz
 Electrical Engineering, M.S.
 Carnegie Mellon University
 Pittsburgh, PA
 emountz@andrew.cmu.edu

Abstract—We optimized the design of an acousto-optic beam steering interdigitated transducer (IDT) design with ScAlN in COMSOL Multiphysics. The simulation material setup was verified with previous literature, and the final simulations considered electromechanical interactions and were conducted in 3D with one IDT unit cell. The data-intensive scope of the simulation necessitated the use of batch processing. The volume of data from the simulations was significantly compressed with an automated post-processing pipeline, including a server/client set-up between COMSOL and MATLAB scripts for classifying results. The results of this simulation study will be tested in a fabricated device. Future efforts include adding the optical simulation to the IDT electromechanical simulation.

I. INTRODUCTION

Acoustic modulation of light introduces a solid-state solution for laser scanning sensors, display technologies, and novel photonic communication technologies. Acoustic modulation exploits the piezoelectric effect to generate periodic and programmable deformation patterns which propagate through a material, negating the need for a control scheme to enable individual pixel control. The acoustic wavelength determines the pitch of the resulting diffraction grating. The angle at which incident light diffracts is a function of the acoustic wavelength. Therefore, broadband interdigitated transducers, which generate the acoustic wave within a piezoelectric material, are critical devices for compact and affordable acousto-optic beam steering devices (Figure 1).

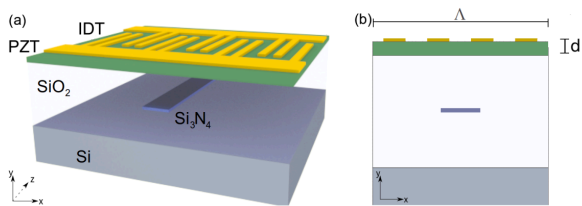


Figure 1. Research on acoustically modulated beam steering devices has explored many different material stack-ups [1]. Our study constructs the IDT electrode fingers out of Aluminum, the piezoelectric material underneath the electrodes (green) in ScAlN, an SiO2 layer with a buried waveguide (similar to that depicted in the figure), and a Silicon substrate.

The electromechanical coupling coefficient relates the effect of the input voltage waveform on the mechanical deformation of the material. The coupling coefficient can be calculated with the following equation:

$$k^2 = \frac{2*(f_r - f_a)}{f_r}$$

where f_r is the resonant frequency and f_a is the antiresonant frequency. The resonant frequency is identified as a local maximum in admittance across the input terminals when the terminals are shorted (at the same potential). The antiresonant frequency is identified as a local minimum admittance across the input terminals of the device in an ‘open’ state (one terminal floating). The magnitude of the electromechanical coupling coefficient is represented by the frequency shift between the resonant and antiresonant frequencies in the ‘short’ versus ‘open’ configurations.

There is a resonant and antiresonant frequency for each electromechanically induced mode, which appear as inverted periodic functions in the deformation pattern of the material. There are multiple electromechanically induced modes. Electromechanically induced modes with surface acoustic waves (SAW) are of interest because they focus the electromechanical energy within the region of the buried waveguide. Rayleigh and Sezawa SAW modes, which have been demonstrated to have useful electromechanical coupling coefficients, will be the focus of this study.

The intent of the study is to optimize the device parameters for maximizing the electromechanical coupling coefficient. The device is a stack of SiO2 and ScAlN on a silicon substrate. The ScAlN is piezoelectric, and thus is directly under the electrodes. The ScAlN is a worthwhile material to study as it is a relatively new and promising alternative to AlN. ScAlN demonstrates a larger piezoelectric coupling coefficient than pure AlN [2]. A layer of SiO2 beneath the ScAlN provides a layer for an optical waveguide. The parameters to be optimized are the thicknesses of the ScAlN (h_{ScAlN}) and the SiO2 (h_{SiO2}), as well as the pitch of the electrodes, which is half of the acoustic wavelength ($\Lambda/2$). The layer thickness parameters are often characterized as ratios of the acoustic wavelength, since it is the relative size of the device which determines the coupling.

II. METHODOLOGY

A. Replication of Previous Works

The calculation of the electromechanical coupling coefficient is carried out with COMSOL Multiphysics simulation, which sweeps the frequency for an admittance analysis, and identifies the mechanical eigenmodes in the structure. We validated the IDT simulation set-up in COMSOL using previous similar published works.

M. Aslam, et al. [3] looked at a similar configuration using COMSOL Multiphysics, with terminals on an AlN layer, directly above an SiO2 layer with a silicon substrate. In a 2D replication of the study, the simulated relationships between acoustic velocity and electromechanical coupling with the thickness of AlN and SiO2 aligned well with the previous literature results (see Figures 2-5). There is a slight

shift in simulated versus published coupling coefficient parameter sweeps. The replication study traded off some mesh quality for speed of simulation and post-processing, so the difference in mesh quality could contribute to the difference in solver solutions.

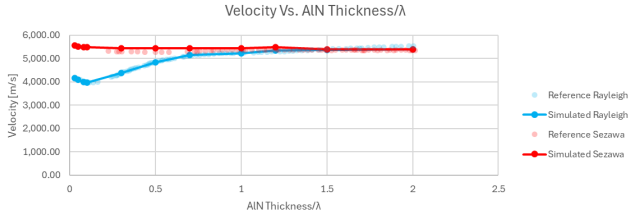


Figure 2. Acoustic wave velocity vs. $h\text{AlN}/\lambda$.

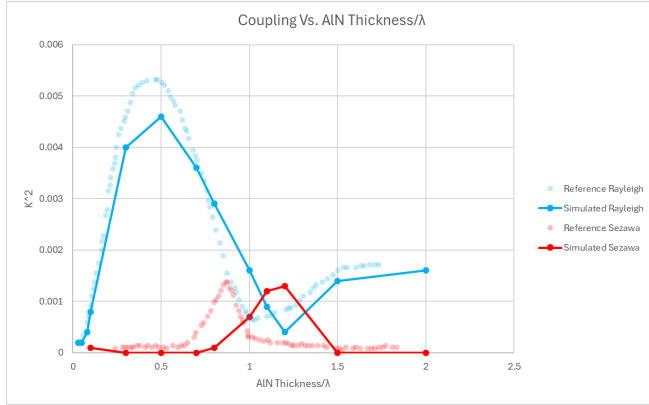


Figure 3. Electromechanical coupling vs. $h\text{AlN}/\lambda$.

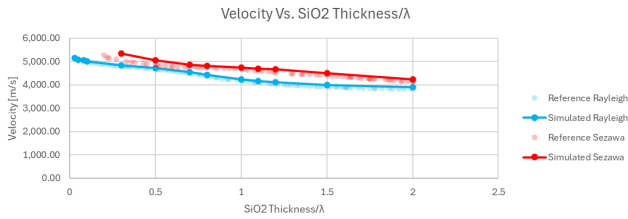


Figure 4. Acoustic wave velocity vs. $h\text{SiO}_2/\lambda$.

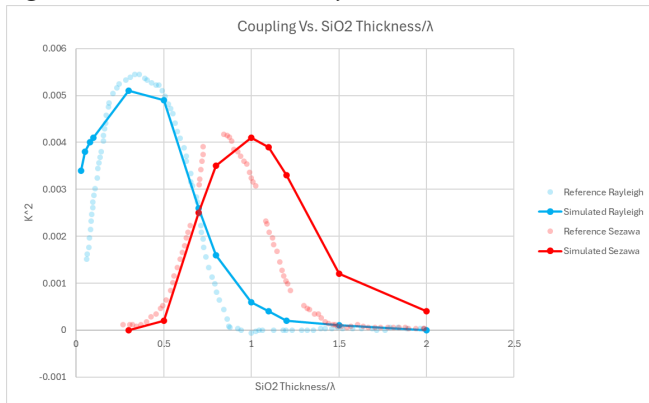


Figure 5. Electromechanical coupling vs. $h\text{SiO}_2/\lambda$.

For our own IDT design study, we analyzed ScAlN instead of AlN. ScAlN in particular has been an active area of research for its promising piezoelectric potential and compatibility with established fabrication methods. We performed our analysis with the ScAlN properties (32% Sc concentration) reported in O. Ambacher, et al. [2]. We used the anisotropic parameters for Silicon that are reported in B. A. Auld, et. al [4], and all other materials were modeled with COMSOL provided default materials.

B. Simulation Geometry

The IDT was designed with Aluminum electrodes on a ScAlN piezoelectric layer. An SiO₂ layer under the ScAlN would contain the buried waveguide for the optical mode, with a silicon substrate. The model includes a layer of air and a perfectly matched layer (PML) to eliminate acoustic reflections from within the substrate (Figure 6).

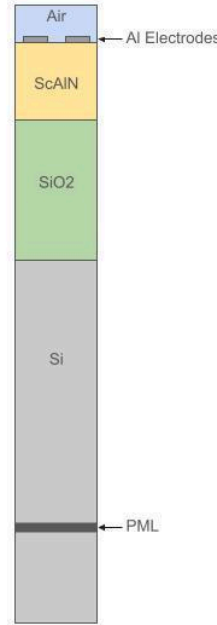


Figure 6. Model geometry.

Charge conservation applies to all materials except the ScAlN, which has a specialized piezoelectric charge conservation model. All materials have an initial voltage of 0V, and the Aluminum terminals are set to GND/GND potential for ‘short’ condition, and GND/Floating potential for ‘open’ condition. The side boundaries are again periodic in the electrical domain. The edges of the Aluminum terminals are modeled in the electrical domain, but the volume of the terminals themselves are not included (assumed perfect conduction within terminals).

Mesh sizing was determined with a mesh convergence study. The meshing of the model must respect the periodic boundary conditions set on the edges. Therefore, the mesh for the side faces of the IDT unit cell are defined with a distribution that is densest at the ScAlN and SiO₂ layers and sized $<0.02\mu\text{m}$, then copied across the two sides of the unit cell. The mesh for the faces of the SiO₂ and ScAlN are fixed to a maximum of $0.02\mu\text{m}$, and the remaining faces are automatically sized. The minimum element quality is 0.1625.

The study compares the electromechanical coupling coefficient across a parametric sweep in order to optimize the device dimensions (See Table 1).

Parameter	Sweep Range (min:increment:max)
$h\text{ScAlN}$	300:50:600nm
$h\text{SiO}_2$	0.5:0.5:1.5 μm
λ	0.5:0.05:1.0 μm
$h\text{ScAlN}/\lambda$	0.3:1.2
$h\text{SiO}_2/\lambda$	0.5:1.5

Table 1. Parametric Sweeps used in the IDT design simulation.

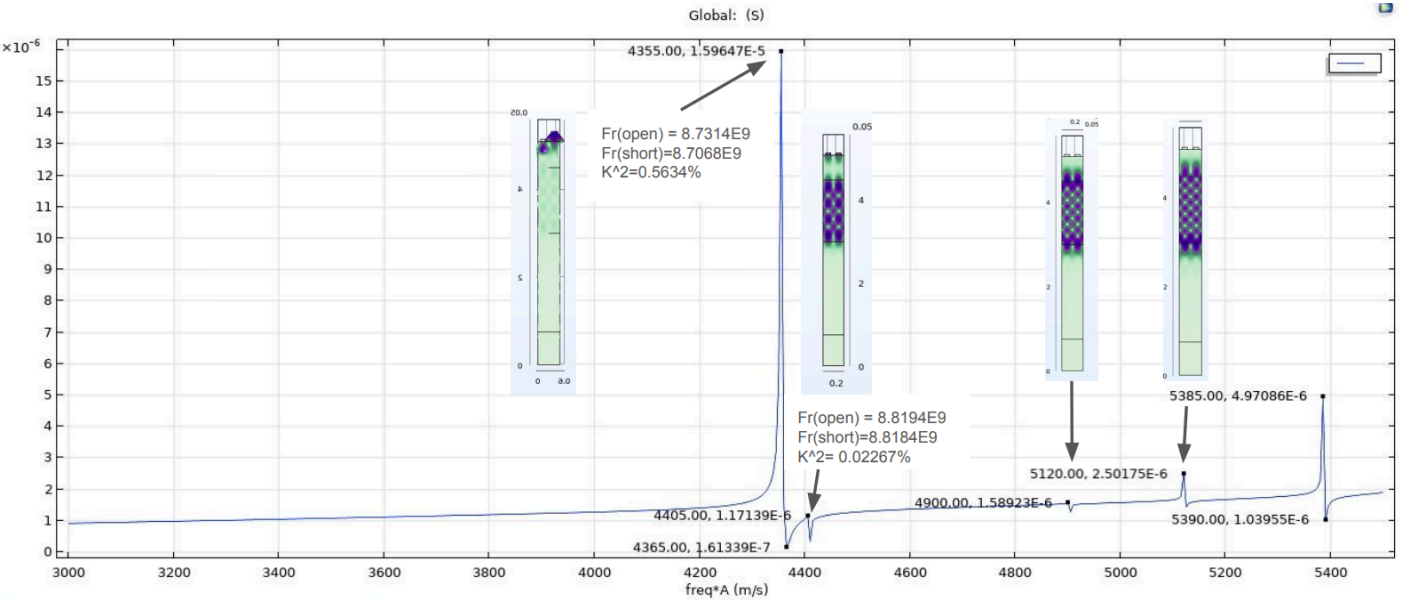
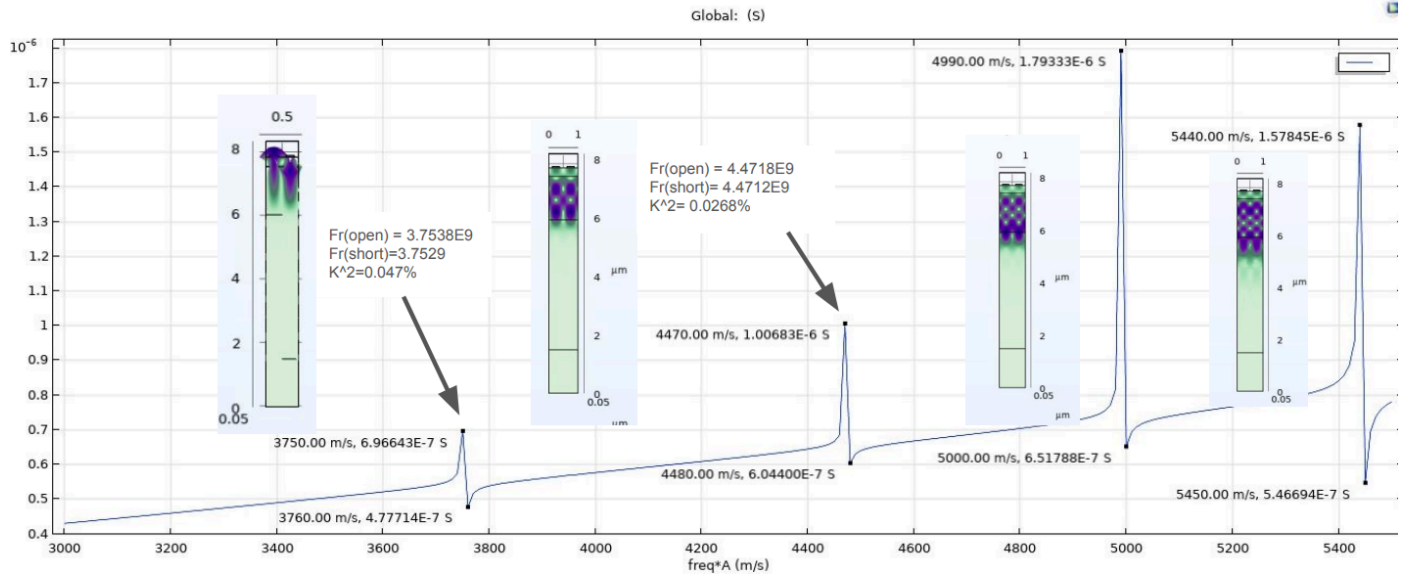


Figure 7. Admittance vs. frequency of input signal applied to terminals. The top plot represents the minimum extreme of $hScAlN/A$ (0.3). The bottom plot represents the maximum extreme (1.2). The local maximum and minimum admittance points are electromechanically coupled resonant and antiresonant modes. The associated eigenmode displacement plots are displayed next to their respective admittance peak. Each admittance peak is labeled with acoustic velocity (m/s), admittance. The resonant frequency (Hz), antiresonant frequency (Hz), and calculated coupling coefficients (%) are also labeled by their respective admittance peaks, with the Rayleigh mode displayed as the first peak, and Sezawa mode at the second peak (study does not analyze peaks above Sezawa frequency).

C. Simulation Configurations

The studies were conducted in 3D with a parametric sweep including 180 permutations, so careful configuration of computational resources was crucial for timely results. The output of the eigenfrequency analysis per parametric configuration was a deformation plot for up to 20 mechanical eigenmodes identified within the input frequency range, and their respective frequencies (~3600 plots total). A post-processing pipeline accessed each of these deformation plots and frequencies in order to parse the electromechanical modes, and then filter the surface acoustic wave modes. A batch sweep allowed the parallelization of simulations for each parameter

configuration to speed up the simulation time. Furthermore, the batch processing returned the results for each parametric configuration in an individual file. These files, which contained the eigenmode deformation plots and frequencies for each parametric configuration, were more manageable to handle in the post-processing pipeline than having a conglomerate file with the results from multiple parametric configurations.

D. Frequency Sweep

First, we performed a frequency sweep at the extremes of the parametric sweep in order to roughly identify the eigenmodes of interest (Rayleigh and Sezawa, Resonant and Antiresonant) (see Figure 7). The frequency

sweep simulates a sinusoidal input at the electrodes of the device, and therefore isolates the electromechanical modes as the local maximum/minimum admittance points. The Rayleigh mode was identified with maximum deflection at the electrodes and attenuating energy in the SiO₂ layer (the first admittance peak in Figure 7). The Sezawa mode was identified with periodic deflection within the SiO₂ (the second admittance peak in Figure 7). Eigenfrequencies of higher frequencies included higher order harmonic deflection patterns within the SiO₂ - we identified the Sezawa mode as the lowest fundamental and did not consider the higher frequency electromechanical modes.

E. Eigenmode Analysis

Once an estimate of the frequencies and electromechanical modes for the device were attained, we conducted a parametrically swept eigenmode analysis within the relevant range of frequencies. The eigenmode analysis was executed for each parametric configuration, in both the ‘short’ and ‘open’ configurations to identify the resonant and antiresonant modes respectively. The results of this analysis are the deformation plots and eigenfrequencies of each eigenmode within the specified frequency range. These eigenmodes include many uninteresting modes, which are purely mechanical and have no electromechanical coupling. First the electromechanical modes had to be identified. Then, the Sezawa and Rayleigh modes had to be identified visually using the deformation plots. Once the resonant and antiresonant modes are identified, the electromechanical coupling coefficient can be calculated for each parametric configuration.

F. Automated Results Analysis

The results of the eigenmode analysis were automatically filtered and sorted using LiveLink, which establishes a client/server connection between COMSOL Multiphysics and MATLAB.

A MATLAB script first identifies resonant/antiresonant modes as the unique frequencies between the ‘open’ and ‘short’ configurations (within some tolerance). This isolates just the modes which exhibit electromechanical coupling, which exhibit frequency translation between the ‘open’ and ‘short’ configurations. The results are further filtered for only SAW modes (excludes modes which do not have maximum deflection within the SiO₂ and ScAlN layers). Finally, the modes are classified as either Rayleigh or Sezawa depending on the maximum integrated deformation being in the ScAlN or the SiO₂. The deformation plots of this filtered selection of eigenmodes is saved for manual quality inspection.

The frequencies at the filtered Rayleigh and Sezawa modes are saved so that the acoustic velocities and coupling coefficients can be calculated automatically.

III. RESULTS

We found that the maximum coupling coefficient of the Rayleigh mode is 0.58%, which is marginally greater than the maximum Sezawa coupling coefficient of 0.5485%. We identified the maximum Rayleigh mode electromechanical coupling with a ScAlN thickness to acoustic wavelength ratio ($hScAlN/\Lambda$) of 1.2, and a SiO₂ thickness to acoustic wavelength ratio ($hSiO_2/\Lambda$) of 1 (See Figures 8-10). The coupling coefficient saturates with $hScAlN/\Lambda$ at about 1,

with marginal gains above (see Figure 8). The coupling coefficient is periodically related to $hSiO_2/\Lambda$, with peaks at harmonics of 1:1 (see Figure 9). The relationships between the parametric configurations and acoustic velocity are explored in the Appendix.

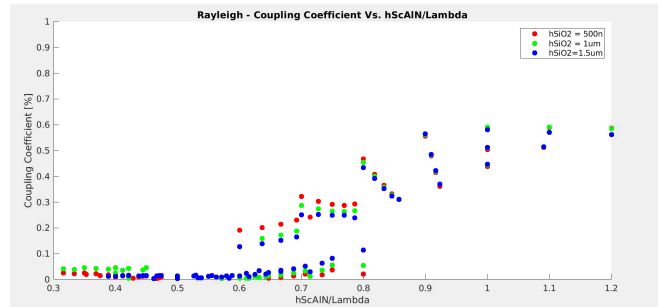


Figure 8. Rayleigh mode coupling coefficient vs. $hScAlN/\Lambda$, color-coded by $hSiO_2$.

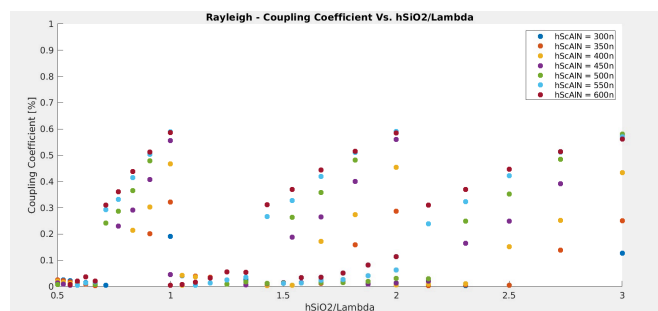


Figure 9. Periodic relationship between Rayleigh mode coupling coefficient vs. $hSiO_2/\Lambda$, color-coded by $hScAlN$.

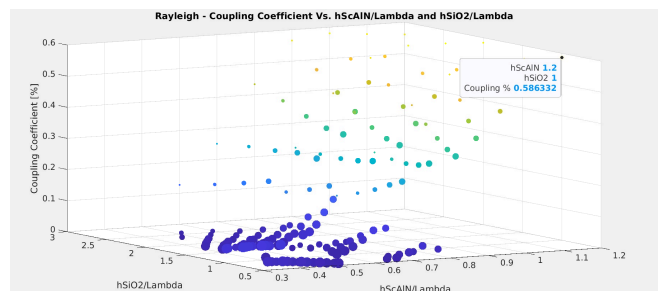


Figure 10. 3D plot of Rayleigh mode coupling coefficient vs. $hSiO_2/\Lambda$ and $hScAlN/\Lambda$.

The Sezawa mode coupling coefficient peaks at 0.5485% with $hScAlN/\Lambda=0.6875$ and $hSiO_2/\Lambda=0.625$ (See Figures 11-13). The relationships between the parametric configurations and acoustic velocity are explored in the Appendix.

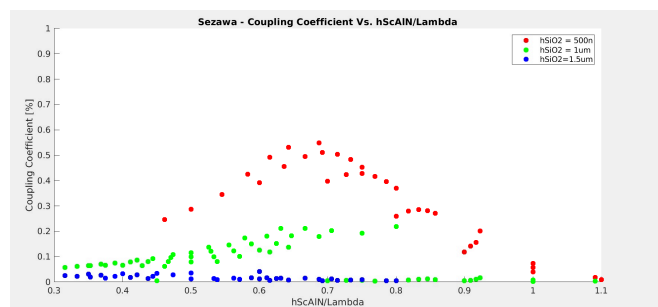


Figure 11. Sezawa mode coupling coefficient vs. $hScAlN/\Lambda$.

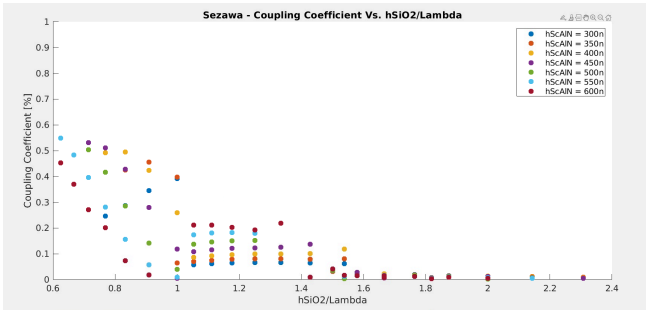


Figure 12. Sezawa mode coupling coefficient vs. $hSiO_2/\Lambda$.

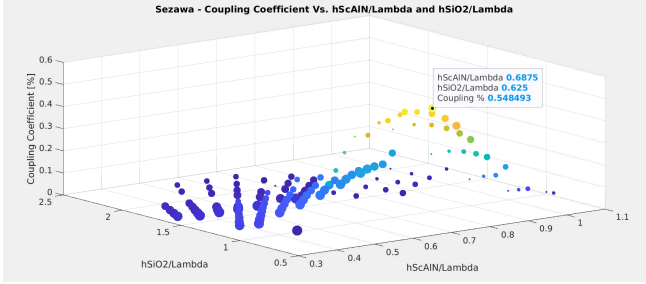


Figure 13. 3D plot of Sezawa mode coupling coefficient vs. $hSiO_2/\Lambda$ and $hScAlN/\Lambda$.

We conducted a brief study on the Rayleigh mode coupling coefficient of the models without the SiO₂ layer, which places the ScAlN directly on the Silicon and did observe improved electromechanical coupling. The Rayleigh mode maximum coupling was 0.5864% with $hScAlN/\Lambda=1.1$ (see Figure 14). The relationship between $hSiO_2/\Lambda$ and velocity without the SiO₂ layer is explored in the Appendix.

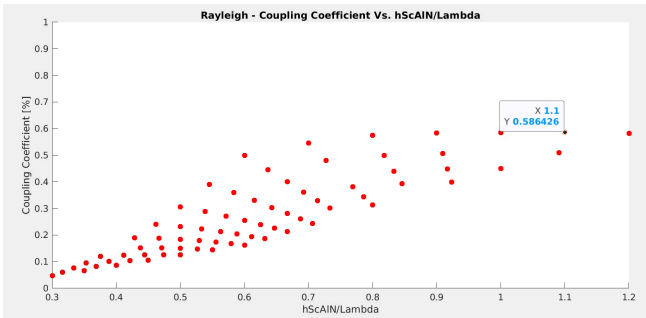


Figure 14. Rayleigh mode coupling coefficient vs. $hScAlN/\Lambda$ for device without SiO₂ layer.

Finally, we directly measured the capacitance between the electrodes of the IDT unit cell in simulation over the parametric sweep (Figure 15). The capacitance increases with $hScAlN$, saturating at about 500nm. The capacitance is not correlated with $hSiO_2$. The capacitance increases with shorter acoustic wavelength (i.e. smaller pitch between the fingers).

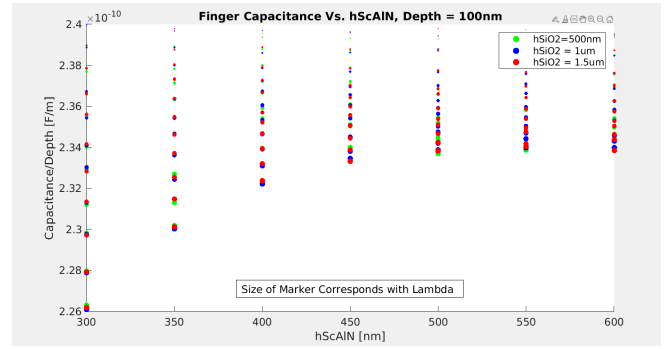


Figure 15. Capacitance between device electrodes vs. $hScAlN$.

IV. CONCLUSION

The maximum coupling coefficient in this study is achieved in the Rayleigh mode with $hScAlN/\Lambda$ equal to 1.2, and $hSiO_2/\Lambda$ equal to 1. However, these dimensions are the upper bounds of parametric sweep. A larger parametric sweep range may improve the electromechanical coupling.

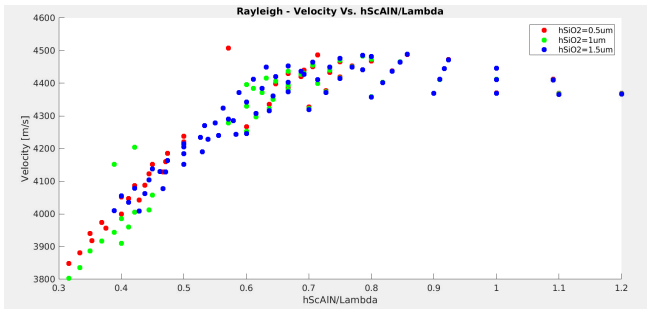
This study does not yet include optical modeling. The coupling coefficient does not consider the location of the buried waveguide. Therefore, the Sezawa mode, which reaches further into the SiO₂ layer where the waveguide is buried, may have a larger electro-optic effect than the Rayleigh.

We did find an improved electromechanical coupling coefficient with the ScAlN directly placed on Silicon, which increases the acoustic wave velocity. Further studies could consider this configuration, perhaps with the SiO₂ and buried waveguide above the ScAlN and electrodes instead of below.

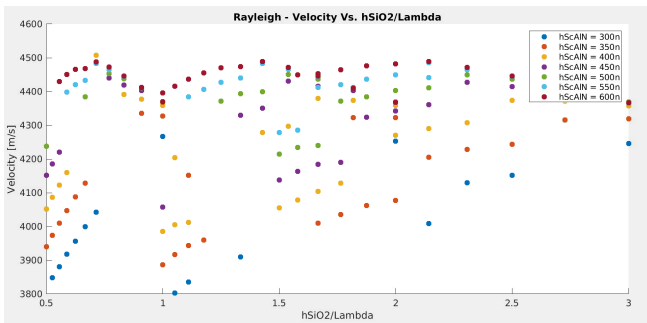
V. REFERENCES

- [1] Peter J. M. van der Slot, Marco A. G. Porcel, and Klaus-J. Boller, "Surface acoustic waves for acousto-optic modulation in buried silicon nitride waveguides," *Opt. Express* 27, 1433-1452 (2019)
- [2] O. Ambacher, B. Christian, N. Feil, D. F. Urban, C. Elsässer, M. Prescher, L. Kirste; Wurtzite ScAlN, InAlN, and GaAlN crystals, a comparison of structural, elastic, dielectric, and piezoelectric properties. *J. Appl. Phys.* 28 July 2021; 130 (4): 045102. <https://doi.org/10.1063/5.0048647>
- [3] Aslam, M.Z.; Jeoti, V.; Karuppanan, S.; Malik, A.F.; Iqbal, A. FEM Analysis of Sezawa Mode SAW Sensor for VOC Based on CMOS Compatible AlN/SiO₂/Si
- [4] Auld, B.A. (1973). *Acoustic fields and waves in solids*. Wiley.

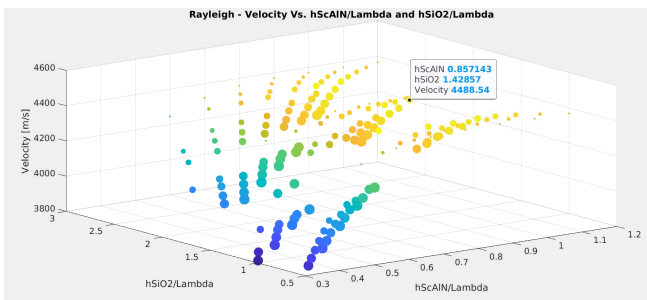
VI. APPENDIX



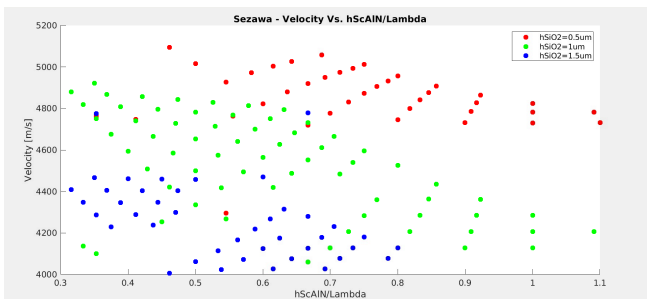
The Rayleigh mode acoustic velocity of the launched wave vs. $hScAlN/\lambda$, which saturates around 0.75. $hSiO_2$ has no significant effect.



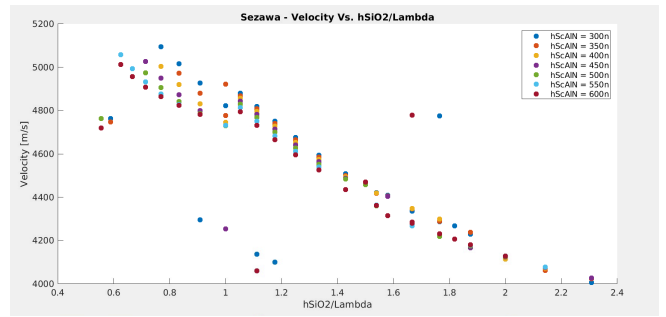
The Rayleigh mode acoustic velocity of the launched wave vs. $hSiO_2/\lambda$. The velocity has a periodic relationship with $hSiO_2/\lambda$ and has a direct relationship with $hScAlN$.



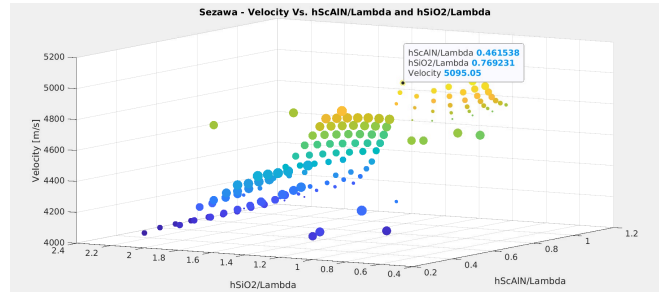
3D plot of logarithmic relationship between Rayleigh mode velocity vs. $hSiO_2/\lambda$ and $hScAlN/\lambda$. Velocity peaks at 4488.54m/s with a $hScAlN/\lambda=0.85$ and $hSiO_2/\lambda=1.42$.



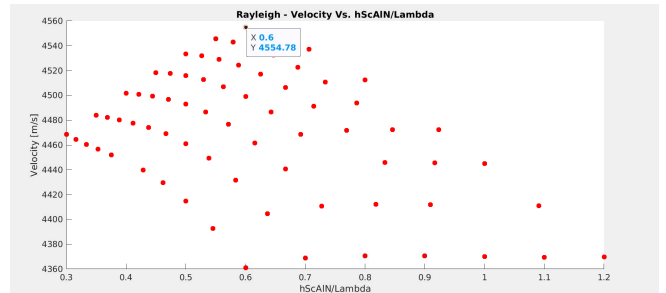
Sezawa mode velocity vs. $hScAlN/\lambda$. Sezawa mode velocity is apparently independent of $hScAlN/\lambda$, and negatively correlated with $hSiO_2/\lambda$.



Strong negative correlation exists between Sezawa mode velocity and $hSiO_2/\lambda$.



3D plot of relationship between Sezawa mode velocity vs. $hSiO_2/\lambda$ and $hScAlN/\lambda$. Velocity peaks at 5095.05m/s with a $hSiO_2/\lambda=0.77$ and $hScAlN/\lambda=0.46$.



Rayleigh mode velocity Vs. $hScAlN/\lambda$ for devices without SiO_2 layer, which places the $ScAlN$ directly on the silicon substrate.